Electronic Supplementary Material (ESI) for Inorganic Chemistry Frontiers.

Nitrogen and boron co-doped metal-free carbon electrocatalyst for efficient oxygen reduction reaction

(Supporting Information)

Yunjie Zhou,[§] Yue Sun,[§] Huibo Wang, Chen Zhu, Jin Gao, Dan Wu, Hui Huang*, Yang Liu*, and Zhenhui Kang*

Jiangsu Key Laboratory for Carbon-based Functional Materials and Devices, Institute of Functional Nano and Soft Materials (FUNSOM), Soochow University, Suzhou, China.

This word file includes:

Electrochemical Measurements.

Figure S1 to S14

Table S1

References

1. Electrochemical Measurements.

1.1 Calculation of electron transfer number (n).

Based on the RDE data, Koutechy-Levich equation was used to determine the numbers of electron transferred per oxygen molecule:[1,2]

$1/j = 1/j_k + 1/B\omega^{1/2}$ (1)

j_k is the measured current density, and ω is the rotation speed of electrode with rpm. B is determined from the slope of the Koutechy-Levich (K-L) plots according to the Levich equation as given by:[3,4]

$B = 0.2nFD_{o2}^{2/3}\upsilon^{-1/6}C_{o2}$ (2)

where n represents the electron transferred number for ORR, F is the Faraday constant ($F = 96{,}485\ C\ mol^{-1}$), D is the diffusion coefficient of O_2 in the 0.1 M KOH solution ($D_{O2} = 1.9\times10^{-5}\ cm^2\ s^{-1}$), υ is the kinetic viscosity in 0.1 M KOH solution ($\upsilon=0.01\ cm^2\ s^{-1}$), C is the bulk concentration of O_2 in the 0.1 M KOH solution ($C_{O2} = 1.2\times10^{-6}\ mol\ cm^{-3}$), and the constant 0.2 is adopted when the rotation speed is expressed at rpm. The K–L plots obtained at different potentials of 0.2, 0.3, 0.4 and 0.5V.

For the RRDE measurements, electrodes were prepared by the same method as for

RDE. The disk electrode was scanned at a rate of 10 mV s^{-1}, and the ring potential was constant at 1.5 V.

$n = 4I_d/(I_d + I_r/N)$ (3)

The $\%HO_2^-$ produced in alkaline solution was calculated by the following equation:[5-7]

$\%HO_2^- = 100 * (2I_r/N) / (I_d+I_r/N)$ (4)

I_d is disk current, I_r is ring current, and N = 0.43 is the current collection efficiency of the Pt ring.

1.2 Test of Electrochemical Active Surface Area.

The electrochemical active surface area (ECSA) for each system was estimated from the electrochemical double-layer capacitance of the NBC-1000. To measure double-layer charging via CV, a potential range in which no apparent Faradaic processes occur was determined from static CV. The range is typically a 0.1 V potential window centered at the open-circuit potential (OCP) of the system. The OCP is -0.05 V vs.SCE in this work, so the range is from -0.1 V to 0 V. The charging current, iC, is then measured from CVs at different scan rates. The double-layer charging current is equal to the product of the scan rate, ν, and the electrochemical double-layer capacitance, C_{DL}, as given by equation: [8-10]

$iC = \nu C_{DL}$ (5)

Thus, a plot of ic as a function of ν yields a straight line with a slope equal to C_{DL}. The ECSA of a catalyst sample is calculated from the double layer capacitance according to equation:

$$ECSA = C_{DL}/Cs \qquad (6)$$

where Cs is the specific capacitance of the sample or the capacitance of an atomically smooth planar surface of the material per unit area under identical electrolyte conditions. For our estimates of surface area, we use general specific capacitances of Cs = 0.022 mF cm^{-2} in 5 M KOH based on typical reported values.[11] The CDL is 0.3236 mF in average as shown in Fig. S4. The ECSA of NBC-1000 was estimated to be 104.0 m^2 g^{-1}.

The electrochemical surface area (ECSA) measurement of 20% Pt/C was tested in Ar-saturated 0.1 M $HClO_4$. The ECSA was calculated by measuring the charge collected in the Hupd adsorption/desorption region after double-layer correction and assuming a value of 0.210 mC cm^{-2} for the adsorption of a hydrogen monolayer (Fig. S5). The ECSA of 20% Pt/C was estimated to be 79.6 m^2 g^{-1}, which is consistent with the study reported.[12]

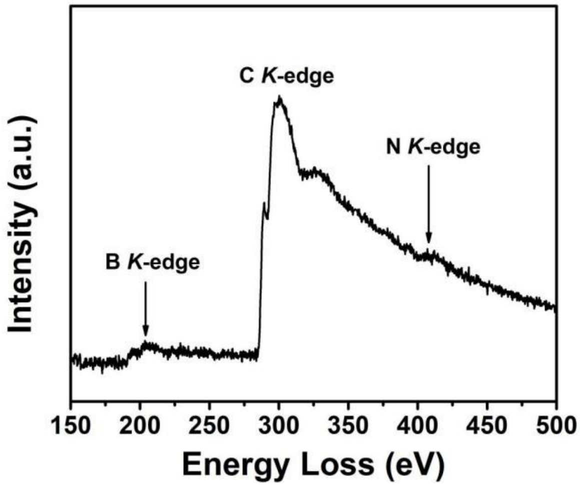

Fig. S1 EEL spectrum of NBC-1000.

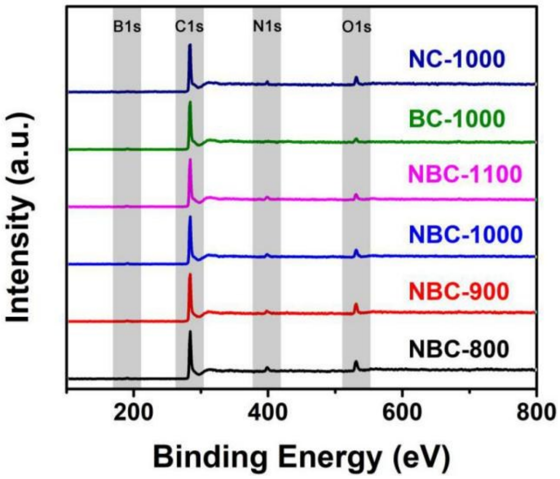

Fig. S2 XPS survey spectra of NBC-800 (black line), NBC-900 (red line), NBC-1000 (blue line) NBC-1100 (pink line), BC-1000 (green line), and NC-1000 (purple line).

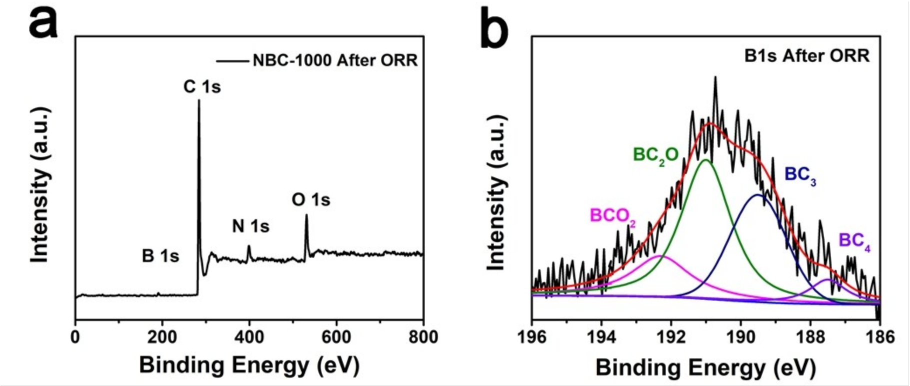

Fig. S3 (a) XPS survey spectra of NBC-1000 after ORR. (b) High resolution B 1s XPS spectra of NBC-1000 after ORR.

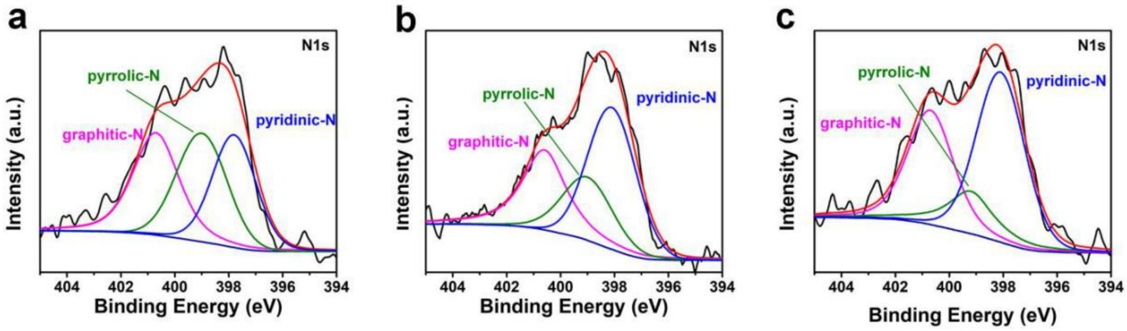

Fig. S4 High resolution N 1s XPS spectra of NBC-800, NBC-900 and NBC-1100.

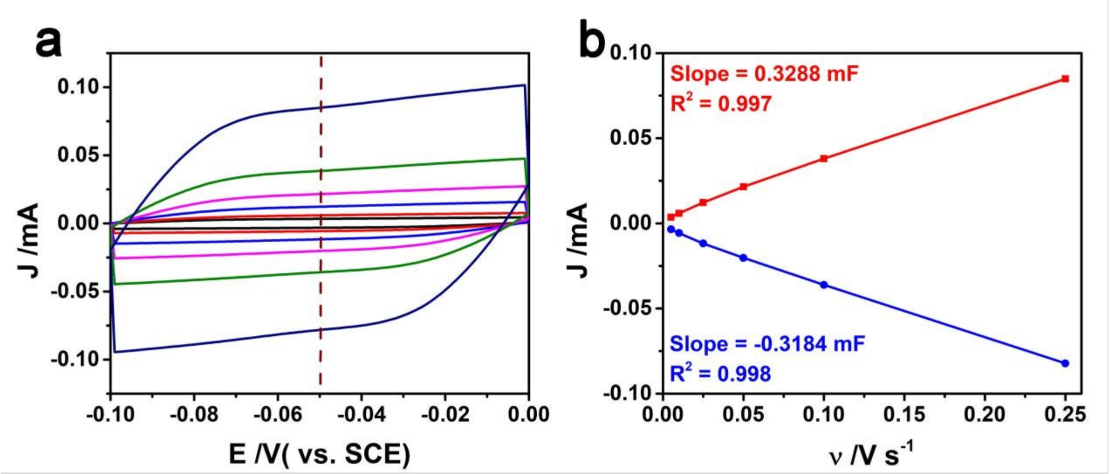

Fig. S5 (A) Cyclic voltammograms were measured in a non-Faradaic region of the voltammogram at the following scan rate: 0.005 (black line), 0.01 (red line), 0.025(blue line), 0.05 (magenta line), 0.1 (olive line), 0.25 (navy line) V/s. The working electrode was held at each potential vertex for 10 s before the beginning the next sweep. (B) The cathodic (red line) and anodic (blue line) charging currents measured at -0.05 V vs SCE plotted as a function of scan rate. The determined double-layer capacitance of the system is taken as the average of the absolute value of the slope of the linear fits to the data.

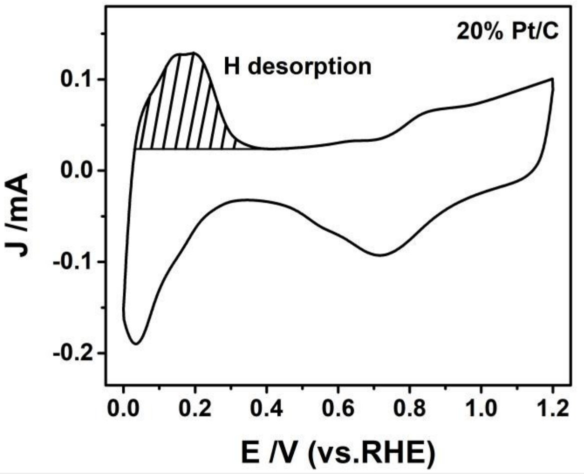

Fig. S6 CV curves of 20% Pt/C. Data was collected at 50mV/s in Ar-saturated 0.1 M $HClO_4$ solution. The hydrogen desorption region from 0.04 V to ~0.4 V vs. RHE was integrated to calculate the ECSA of Pt.

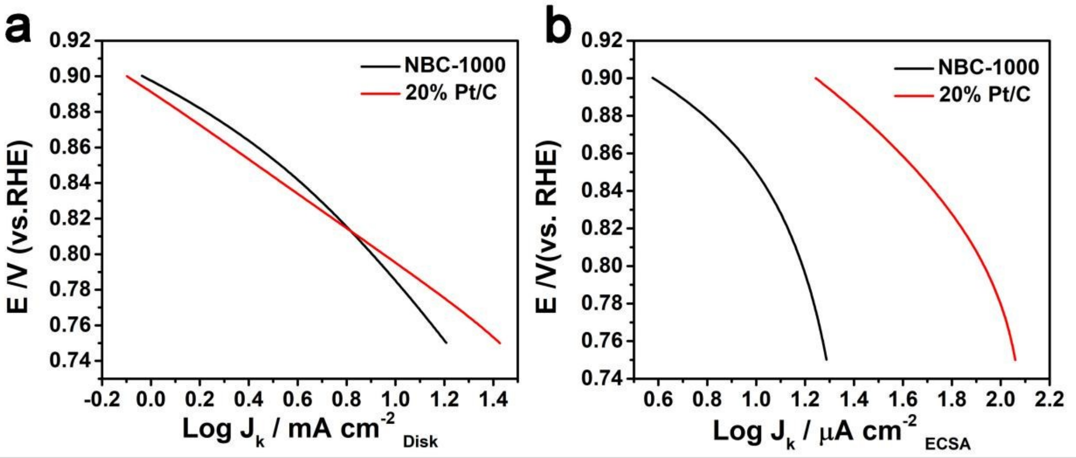

Fig. S7 Tafel plots of ORR activities normalized by geometric surface area of electrodes (disk surface area) (a), and electrochemical surface area (b).

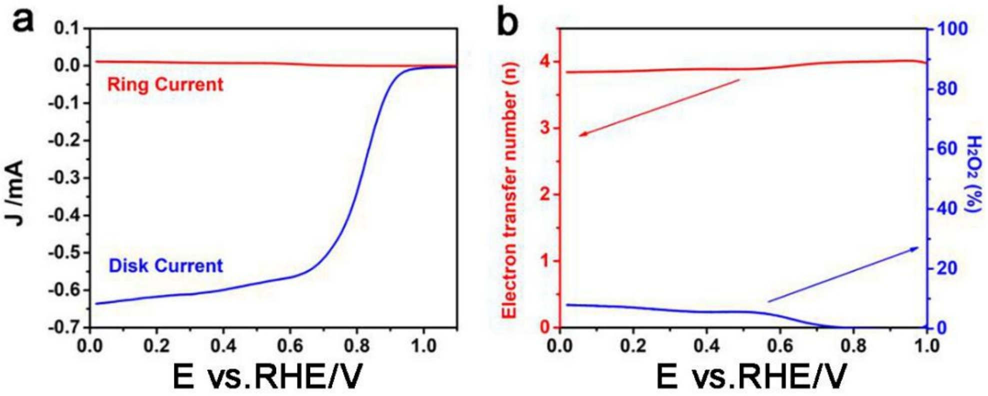

Fig. S8 (a) RRDE tests of NBC-1000 in O_2-saturated 0.1 M KOH at a rotation speed of 1600 rpm with a scan rate of 10 mV/s (The Pt ring electrode was polarized at 1.5 V vs. RHE.). (b) Electron transfer number (n) and peroxide percentage of NBC-1000 within the potential range of 0 V to 1 V vs. RHE.

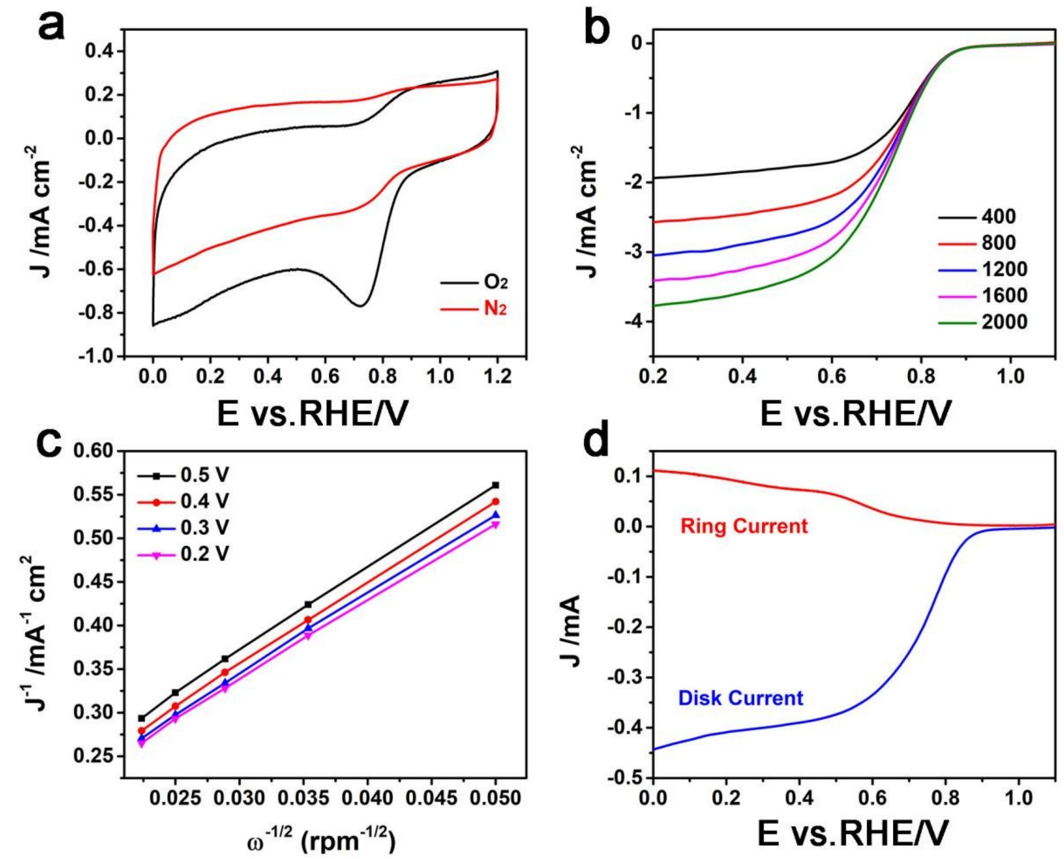

Fig. S9 (a) CV tests of pristine graphene in nitrogen- (Red line) and oxygen- (Black line) saturated 0.1 M KOH solution at a sweeping rate of 50 mV/s. (b) ORR polarization curves of pristine graphene with various rotation rates at a scan rate of 10 mV/s. (c) Koutecky–Levich (K–L) plots of pristine graphene at different electrode potentials. (d) RRDE tests of pristine graphene in O_2-saturated 0.1 M KOH at a rotation speed of 1600 rpm with a scan rate of 10 mV/s (The Pt ring electrode was polarized at 1.5 V vs. RHE.).

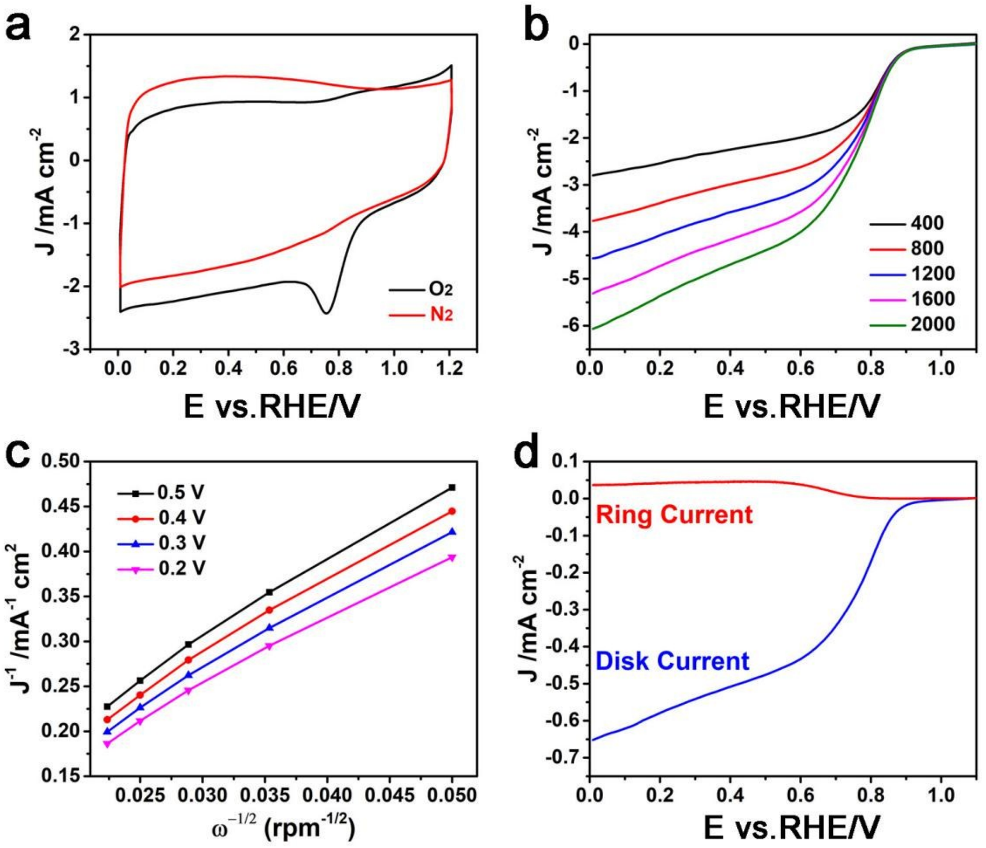

Fig. S10 (a) CV tests of NBC-800 in nitrogen- (Red line) and oxygen- (Black line) saturated 0.1 M KOH solution at a sweeping rate of 50 mV/s. (b) ORR polarization curves of NBC-800 with various rotation rates at a scan rate of 10 mV/s. (c) Koutecky–Levich (K–L) plots of NBC-800 at different electrode potentials. (d) RRDE tests of NBC-800 in O_2-saturated 0.1 M KOH at a rotation speed of 1600 rpm with a scan rate of 10 mV/s (The Pt ring electrode was polarized at 1.5 V vs. RHE).

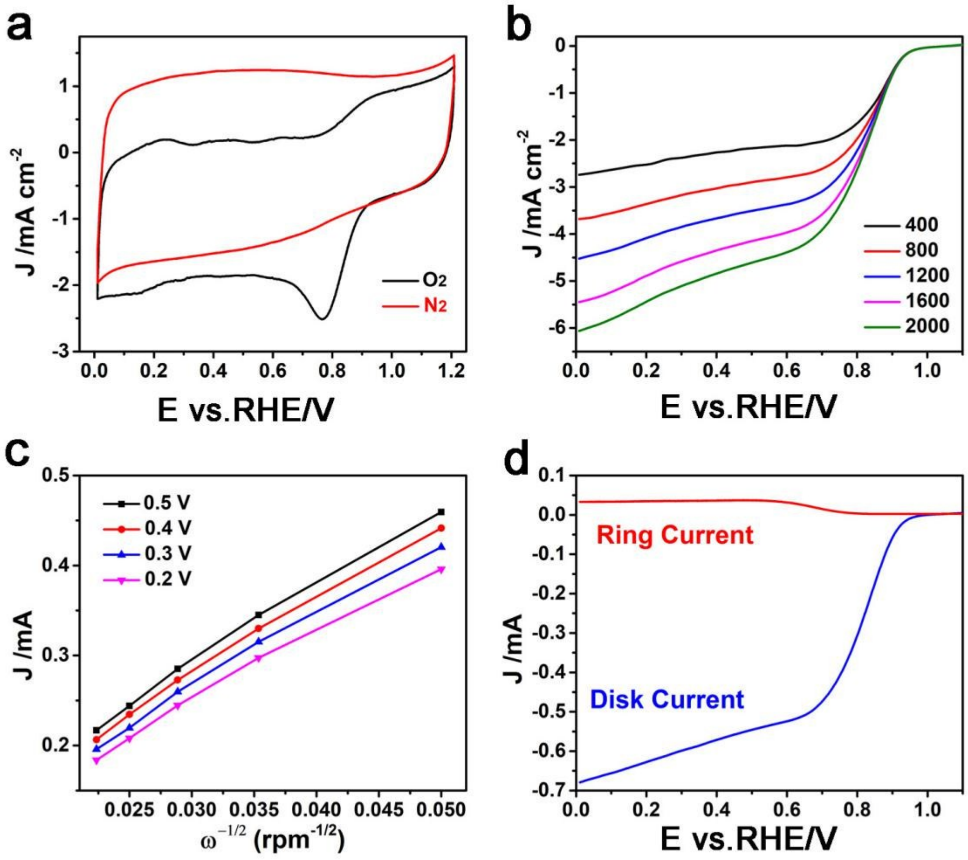

Fig. S11 (a) CV tests of NBC-900 in nitrogen- (Red line) and oxygen- (Black line) saturated 0.1 M KOH solution at a sweeping rate of 50 mV/s. (b) ORR polarization curves of NBC-900 with various rotation rates at a scan rate of 10 mV/s. (c) Koutecky–Levich (K–L) plots of NBC-900 at different electrode potentials. (d) RRDE tests of NBC-900 in O_2-saturated 0.1 M KOH at a rotation speed of 1600 rpm with a scan rate of 10 mV/s (The Pt ring electrode was polarized at 1.5 V vs. RHE).

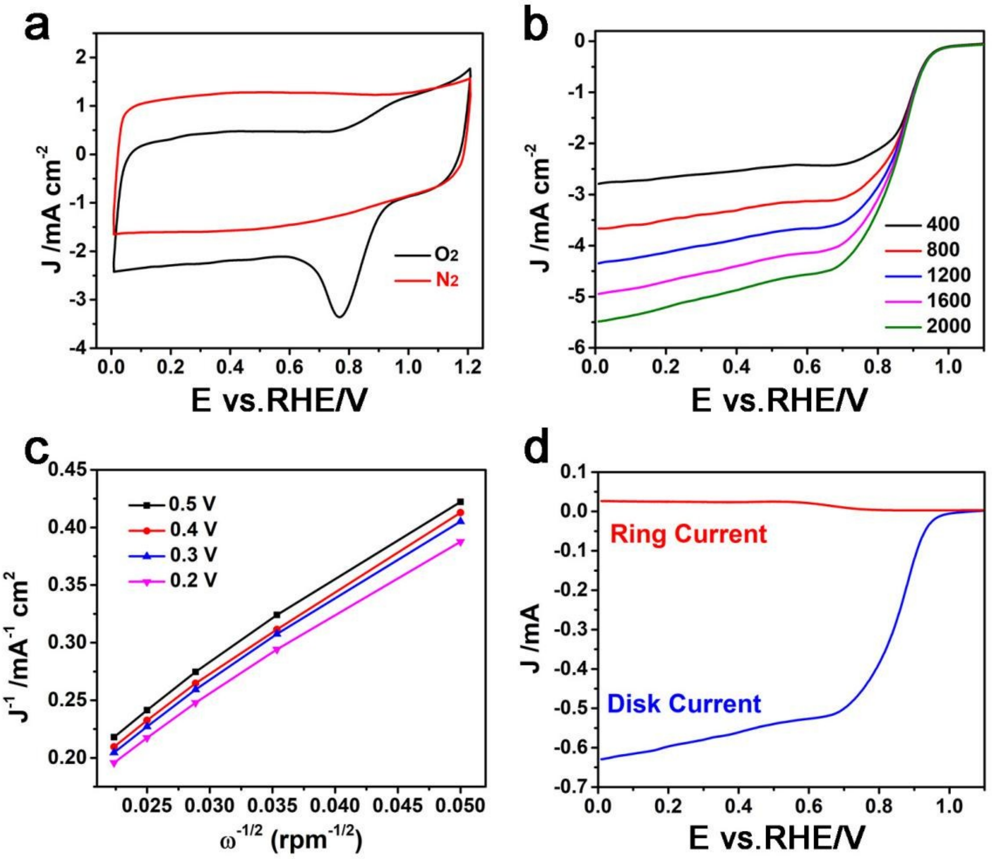

Fig. S12 (a) CV tests of NBC-1100 in nitrogen- (Red line) and oxygen- (Black line) saturated 0.1 M KOH solution at a sweeping rate of 50 mV/s. (b) ORR polarization curves of NBC-1100 with various rotation rates at a scan rate of 10 mV/s. (c) Koutecky–Levich (K–L) plots of NBC-1100 at different electrode potentials. (d) RRDE tests of NBC-1100 in O_2-saturated 0.1 M KOH at a rotation speed of 1600 rpm with a scan rate of 10 mV/s (The Pt ring electrode was polarized at 1.5 V vs. RHE).

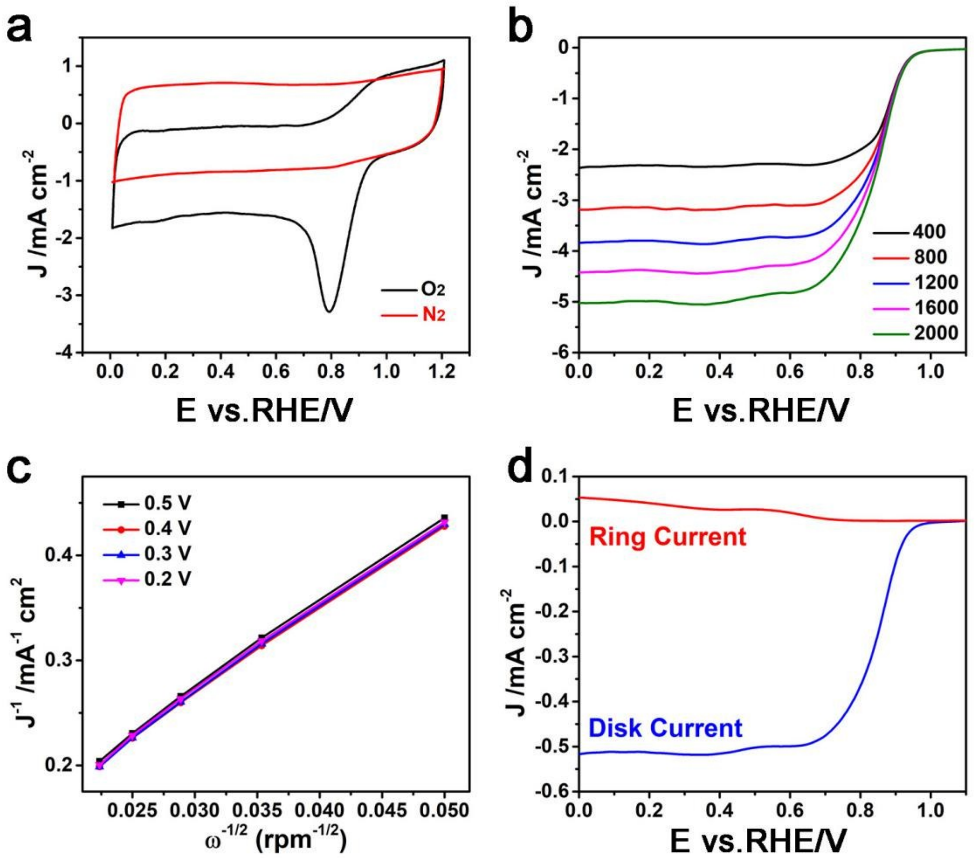

Fig. S13 (a) CV tests of NC-1000 in nitrogen- (Red line) and oxygen- (Black line) saturated 0.1 M KOH solution at a sweeping rate of 50 mV/s. (b) ORR polarization curves of NC-1000 with various rotation rates at a scan rate of 10 mV/s. (c) Koutecky–Levich (K–L) plots of NC-1000 at different electrode potentials. (d) RRDE tests of NC-1000 in O_2-saturated 0.1 M KOH at a rotation speed of 1600 rpm with a scan rate of 10 mV/s (The Pt ring electrode was polarized at 1.5 V vs. RHE).

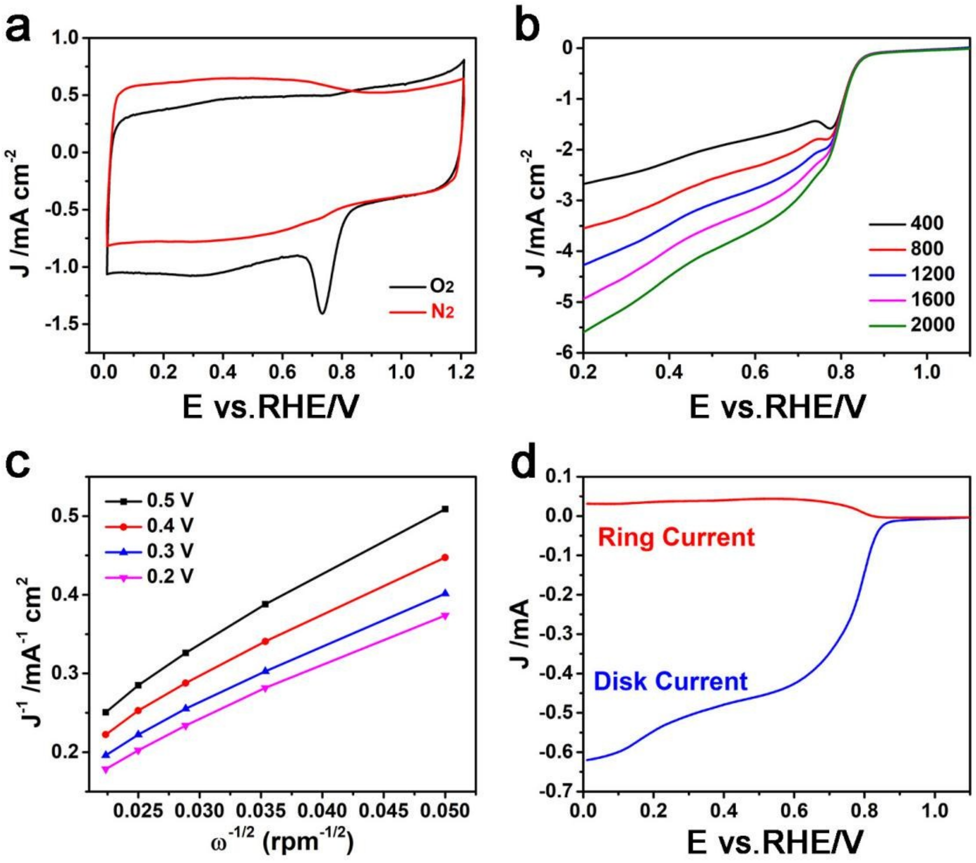

Fig. S14 (a) CV tests of BC-1000 in nitrogen- (Red line) and oxygen- (Black line) saturated 0.1 M KOH solution at a sweeping rate of 50 mV/s. (b) ORR polarization curves of BC-1000 with various rotation rates at a scan rate of 10 mV/s. (c) Koutecky–Levich (K–L) plots of BC-1000 at different electrode potentials. (d) RRDE tests of BC-1000 in O_2-saturated 0.1 M KOH at a rotation speed of 1600 rpm with a scan rate of 10 mV/s (The Pt ring electrode was polarized at 1.5 V vs. RHE).

Table S1. Comparisons of ORR performance with NBC-1000 and other similar catalysts. All values were obtained in alkaline conditions with 0.1 M KOH.

Samples	E_{oneset} (V)	$E_{half\ wave}$ (V)	J_{max} (mA cm^{-2})	electron transfer number (n)	Reference electrode	Ref.
NBC-1000	0.97	0.84	5.40	3.93	RHE	This work
BNC-1000	0.86	0.75	3.68	3.60	RHE	[14]
hCNB-800	0.89	0.8	5.25	3.94	RHE	[15]
BCN-2	0.92	0.82	5.20	3.92	RHE	[16]
NB-HCT	0.93	0.81	4.46	3.60-4.00	RHE	[17]
BND	-0.05	-0.18	5.00	3.96	SCE	[18]
N,B-GA-1000	-0.05	-0.24	6.20	3.90	SCE	[19]
BCN	-0.25	-0.35	2.25	3.43	Ag/AgCl	[20]
BCN-2.5-1000	0.05	-0.15	6.00	3.97	Ag/AgCl	[21]
BNC-800	-0.04	-0.21	5.38	3.83	Ag/AgCl	[22]

Reference:

1 Y. Liang, H. Wang, J. Zhou, Y. Li, J. Wang, T. Regier and H. Dai, *J. Am. Chem. Soc.*, 2012, **134**, 3517–3523.

2 S. K. Zecevic, J. S. Wainright, M. H. Litt, L. Gojkovic and R. F. Savinell, *J. Electrochem. Soc.*, 1997, **144**, 2973–2981.

3 Y. Zhou, Y. Sun, C. Zhu, Y. Liu, X. Dai, J. Zhong, Q. Chen, H. Tian, R. Zhou and Z. Kang, *J. Mater. Chem. A*, 2018, **6**, 8955–8961.

4 O. Antoine and R. Durand, *J. Appl. Electrochem.*, 2000, **30**, 839–844.

5 Y. Liang, H. Wang, J. Zhou, Y. Li, J. Wang, T. Regier and H. Dai, *J. Am. Chem.*

Soc., 2012, **134**, 3517–3523.

6 J. Du, Y. Pan, T. Zhang, X. Han, F. Cheng and J. Chen, *J. Mater. Chem.*, 2012, **22**, 15812.

7 W. Bian, Z. Yang, P. Strasser and R. Yang, *J. Power Sources*, 2014, **250,** 196–203.

8 S. Trasatti and O. A. Petrii, *Pure Appl Chern*, 1991, **63,** 711–734.

9 J. D. Benck, Z. Chen, L. Y. Kuritzky, A. J. Forman and T. F. Jaramillo, *ACS Catal.*, 2012, **2,** 1916–1923.

10 G. Gryglewicz, J. Machnikowski, E. Lorenc-Grabowska, G. Lota and E. Frackowiak, *Electrochimica Acta*, 2005, **50,** 1197–1206.

11 T. A. Centeno and F. Stoeckli, *J. Power Sources*, 2006, **154,** 314–320.

12 X. Xie, Y. Nie, S. Chen, W. Ding, X. Qi, L. Li and Z. Wei, J. Mater. Chem. A, 2015, 3, 13962-13969.

13 M. Li, Z. Zhao, T. Cheng, A. Fortunelli, C. Chen, R. Yu, Q. Zhang, L. Gu, B. Merinov, Z. Lin, E. Zhu, T. Yu, Q. Jia, J. Guo, L. Zhang, W. Goddard III, Y. Huang, X. Duan, *Science*, 2016, **354,** 1414-1419.

14 Y. Qian, Z. Hu, X. Ge, S. Yang, Y. Peng, Z. Kang, Z. Liu, J. Y. Lee and D. Zhao, *Carbon*, 2017, **111**, 641–650.

15 J.-S. Han, D. Y. Chung, D.-G. Ha, J.-H. Kim, K. Choi, Y.-E. Sung and S.-H. Kang, *Carbon*, 2016, **105**, 1–7.

16 H. Tabassum, R. Zou, A. Mahmood, Z. Liang and S. Guo, *J. Mater. Chem. A*, 2016, **4**, 16469–16475.

17 C. Cao, L. Wei, Q. Zhai, G. Wang and J. Shen, *Electrochimica Acta*, 2017, **249**, 328–336.

18 Y. Liu, S. Chen, X. Quan, H. Yu, H. Zhao, Y. Zhang and G. Chen, *J. Phys. Chem. C*, 2013, **117**, 14992–14998.

19 C. Xu, Y. Su, D. Liu and X. He, *Phys. Chem. Chem. Phys.*, 2015, **17**, 25440–25448.

20 S. Lee, Y. Heo, M. A. Bratescu, T. Ueno and N. Saito, *Phys. Chem. Chem. Phys.*, 2017, **19**, 15264–15272.

21 J. Jin, F. Pan, L. Jiang, X. Fu, A. Liang, Z. Wei, J. Zhang and G. Sun, *ACS Nano*, 2014, **8**, 3313–3321.

22 X. Huang, Q. Wang, D. Jiang and Y. Huang, *Catal. Commun.*, 2017, **100**, 89–92.